eV-TEM: transmission electron microscopy with few-eV electrons

Geelen, D.

Chapter 1

Introduction

Electron microscopy has become an extremely important technique in a wide variety of fields. The resolving power is vastly superior to light microscopes and electron microscopy has proven to be valuable in fields ranging from archaeology and geology to biology and condensed-matter physics.

A major disadvantage is that the electron energy used in conventional **E**lectron **M**icroscopy (EM) ranges from 10's to 100's of keV. Such energetic electrons can significantly damage the specimen. This is especially relevant in the study of biological samples and organic materials in general. Major efforts are being made to avoid this radiation damage from interfering with the study of such materials. There are several approaches to minimize damage in EM. These include developing better detectors such that lower electron doses are sufficient to form an image, and lowering the electron energies to several keV.

In this dissertation I present the development of, and measurements with, a transmission electron microscope that uses electron energies five orders of magnitude lower than in conventional **T**ransmission **E**lectron **M**icroscopes (TEMs). The energies we use are in the order of a few eV. Hence, we call our technique 'eV-TEM'.

1.1 The invention of the first electron microscope

The first electron microscope was built by Max Knoll and Ernst Ruska in 1931 in Berlin. Already in 1929, Ruska had observed that when he irradiated a metal film with a small hole in it, he could use magnetic fields as a lens to bend the transmitted electron trajectories in such a way that an image of the hole would be formed by these electrons. This observation inspired Knoll and Ruska to try to use an additional lens to construct a microscope, just like in light optics. A sketch of this configuration is presented in figure 1.1 together with some of their earliest results. They used their electron optics to form an image of platinum grids irradiated with electrons. The microscope had a magnification of just 14.4. For magnifications larger than this, the radiation required to obtain enough contrast to form an image was so high that the molybdenum and platinum specimens would quickly melt. Ruska and Knoll therefore even avoided the use of the term electron microscope. It turned out that their modesty was unnecessary and their prototype is now regarded as the first electron microscope. Ernst Ruska was awarded the 1986 Nobel prize in physics.

1.1.1 Better-than-light microscope

When Ruska and Knoll were working on their first electron microscope prototype, they were aware of the resolution limit in light optics. This was based on the work of Ernst Abbe in 1873 [1] where he found that the maximum resolution achievable with a visible light microscope was limited by the wavelength of light and the angular acceptance of the optical system. Abbe showed that the smallest resolvable distance d is given by what is now called the Abbe diffraction limit:

$$d = \frac{\lambda}{2NA} \tag{1.1}$$

with λ the wavelength of the light used to form an image and NA the numerical aperture of the optical system*. Knoll and Ruska thought this should not be an issue for an electron microscope since they were not using light to image the samples and they hoped electrons to be extremely small. They did not realize

* $NA = n \sin\theta$, where n is the refractive index of the medium in which the lens is embedded and θ is the maximum angle accepted by the lens.

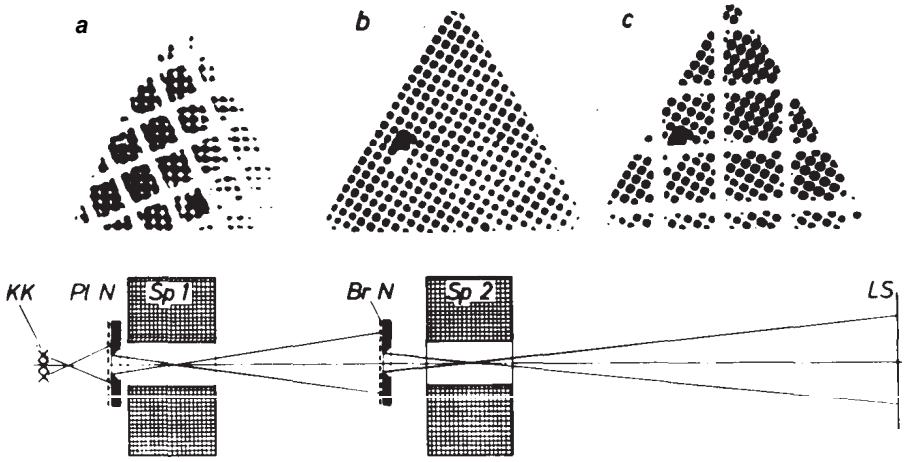

Figure 1.1: First proof (7 april 1931) that something irradiated by electrons can be imaged with two magnetic lenses. (**a**) shows a platinum grid imaged with one coil (coil 1, denoted by Sp 1 in the bottom schematic). (**b**) A bronze grid imaged with one coil (coil 2, denoted by Sp 2). (**c**) Here the images of both the platinum and bronze grids are superposed. The image of the platinum grid is projected on the bronze grid by coil 1. This is then transfered to the fluorescent screen by coil 2. The electron energy used was 50 keV (from Ruska's Nobel lecture December 8, 1986).

that electrons also behave wavelike, just like light. This was first proposed in 1925 by De Broglie and experimentally shown in 1927 by Davisson and Germer, in parallel with George Paget Thomson (for which Davisson and Thomson received the 1937 Nobel prize in in physics). Therefore, the Abbe diffraction limit also applies to imaging with electrons. Ruska only became aware of the work of De Broglie in the summer of 1931. Initially it disappointed Ruska that even electron microscopes are subject to a diffraction limit. But he quickly realized that this is not nearly as restricting as with visible light microscopes. The De Broglie 'matter wavelength', λ, is given by:

$$\lambda = \frac{h}{\sqrt{2mE}} \tag{1.2}$$

λ depends on the electron mass m and the electron energy E, the factor h is Planck's constant. This means that when using 50 keV electrons the electron wavelength, about 5 pm, is five orders of magnitude smaller than that of visible light. Inspired by this, Ruska decided to work on an electron microscope that could surpass the resolution of a light microscope. When we use equation 1.1 with Ruska's angle acceptance of 2×10^{-2} rad, we find that diffraction limits the resolution to 2.7 Å. In 1933 Ruska managed to build the first better-than-light microscope. He was able to make images of cotton fibers. These, however, quickly carbonized due to radiation damage. He found that when the samples were thin enough, an image could also be formed using contrast as a consequence of interference (phase contrast) instead of just absorption. With this the samples heated up much less. Now, about 86 years later, the highest resolution transmission electron microscopes are capable of distinguishing individual atoms with sub-Ångström resolution and can do elemental analysis on the same scale. This became possible because of the development of advanced aberration correction for electron optics.

1.2 High-energy electrons

The key insight that makes TEM such a valuable technique is that with thin enough samples images can be obtained solely by phase contrast instead of just absorption. This dramatically reduces the amount of energy transfered to the sample and therefore the damage.

When the sample is thin enough, the interaction of electrons with the material can be described by considering weak electron scattering from the individual atoms to a very good approximation. Even though this describes the interaction very well, radiation damage does reduce the number of applications TEM can be used for. As a consequence of energy and momentum conservation, there will always be energy transfer when an electron scatters off an atom. In extreme cases, this leads to the removal of atoms from the material [2]. Many materials are not significantly affected by radiation damage and can be easily studied in TEM. However, all materials will be destroyed at some point by high-energy electron imaging.

1.3 Reducing damage

Radiation damage in organic materials is one of the biggest problems in electron microscopy. Here even a small energy transfer can change the molecular configuration or break molecular bonds in the material that is being investigated. This does not mean that TEM cannot be used to study such materials. Radiation sensitive materials can be studied by using advanced techniques. Recently, there has been a lot of development in the detectors used in TEM. There are now direct electron detectors that can detect single electrons. This technique is often referred to as **S**ingle **P**article **E**lectron **M**icroscopy (SPEM) [3]. The idea behind this is that a much smaller electron dose is needed, such that an image can be formed before the sample is significantly damaged. In addition to advances in electron optical aberration correction, there are now TEMs available with atomic resolution that operate with electron energies as low as 10 keV. However, also 10 keV electrons cause damage. Hence, we have chosen a completely different approach.

1.4 Transmission electron microscopy with extremely low-energy electrons

In the energy regime below ~ 50 eV, especially below ~ 10 eV, many of the mechanisms causing damage at high-electron energies are not available [5]. The reduction of the cross section of such mechanisms at low energies implies that the **M**ean **F**ree **P**ath (MFP), which is the average distance an electron

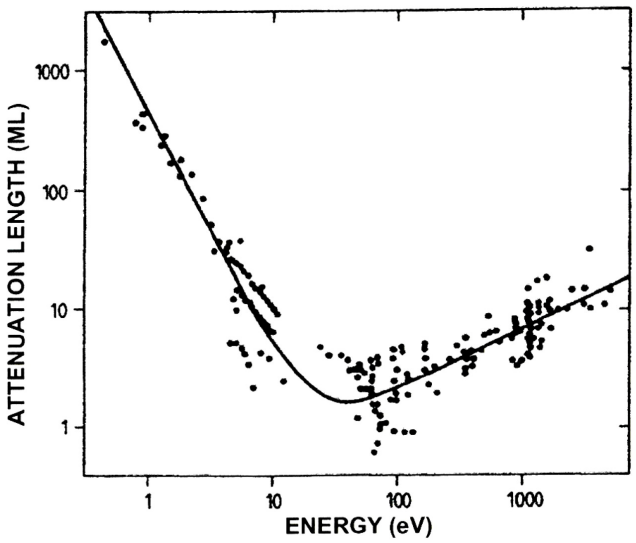

Figure 1.2: The so-called universal curve of the electron mean free path. The electron mean free path is determined for many different materials. This figure is from [4].

travels between scattering events, increases at low energies. This phenomenon is captured in the so-called 'universal curve' for the electron MFP. This summarizes data for a large set of materials, shown in figure 1.2. The universal curve shows that the mean free path of high-energy electrons in a material is long. This is one of the reasons why conventional TEMs use such high-energy electrons. In the high-energy regime the MFP decreases with decreasing energy. This continues down to an energy of about 50 eV, where we find a minimum in the universal curve. Going to even lower energies the MFP starts to increase again. This suggests that materials are increasingly transparent to **L**ow-**E**nergy **E**lectrons (LEE) as electron energy is further reduced.

For this reason, we have developed a TEM that operates in the 0-100 eV energy regime. With this technique we can image materials in transmission, using LEE. Moreover, since we can vary the exact energy of the incoming electrons, it also enables us to perform spectroscopy at low energies. Hence, this new form of TEM combines microscopic with spectroscopic capabilities.

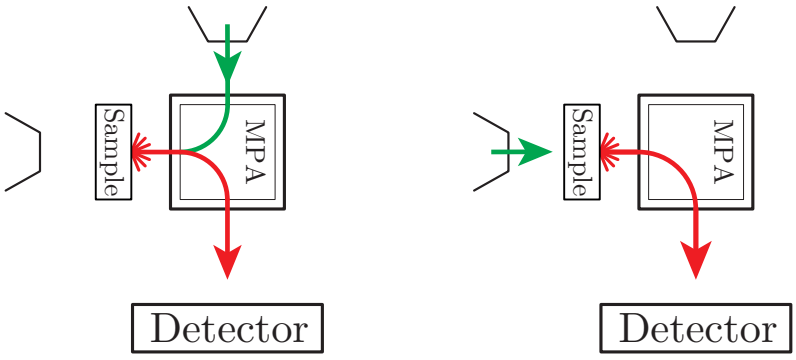

(a) LEEM **(b)** eV-TEM

Figure 1.3: Schematic representation of the reflection-LEEM and eV-TEM. **(a)** Reflection-LEEM: The sample is illuminated from the front (incoming electron beam is indicated by a green arrow) such that an image is formed with reflected electrons (the outgoing electron beam is indicated with a red arrow). Since the electron source and the detector are placed on the same side of the sample, a **M**agnetic **P**rism **A**rray (MPA) is used to separate the incoming and outgoing beam paths. **(b)** eV-TEM: an electron source is placed behind the sample such that an image is formed with transmitted electrons.

To achieve this, we adapted a SPECS P-90 **L**ow-**E**nergy **E**lectron **M**icroscope (LEEM) [6], called the ESCHER instrument. In LEEM, samples are investigated using reflected LEE. A sample is illuminated with electrons originating from an electron gun that is placed on top of the instrument. Here electrons are accelerated to an energy of 15 keV and directed into a so-called **M**agnetic **P**rism **A**rray (MPA), which deflects the electrons towards the sample, see figure 1.3. The sample is kept at a high negative potential, tunable around -15 keV. Electrons are therefore decelerated as they approach the sample and arrive there with an energy that we can accurately control. Upon reflection, the electrons will be accelerated to their original energy of 15 keV back into the MPA, which deflects them into the imaging system. Finally an image (or a diffraction pattern) is formed at the detector.

Since a LEEM instrument is optimized to form images with LEE, irrespective of the way a sample is illuminated, it provides an attractive platform for eV-TEM to be developed. In order to study the transmission of LEEs, we have modified the instrument, by placing a miniature low-energy electron source behind the sample. As the sample is irradiated from the back, transmitted electrons are accelerated into the imaging system. Since the eV-TEM electron source is placed behind the sample, it does not interfere with the original capabilities of the ESCHER instrument and reflection measurements are still possible. Hence, we can detect all electrons leaving the sample and compare the reflected and transmitted signals.

This adaptation of the ESCHER instrument has several interesting consequences. First of all, we can perform electron microscopy in reflection and transmission with little or no damage. Second, we are able to do spectroscopy with both transmitted and reflected LEE. The latter will also provide unprecedented information on electron scattering and absorption, as explained in chapter 5. Having data on both elastic and inelastic electron scattering is important to understand the processes involved in radiation damage, e.g. when imaging organic structures such as DNA with LEE. Interestingly, the relevance of such studies extrapolates beyond LEE only. Loss processes of high-energy electrons or photons can set off a cascade of many lower-energy electrons [7]. Hence, in many cases damage induced by high-energy electrons and even high energy photons is actually governed by the interactions of lower-energy electrons with the material. We are especially interested in the

latter phenomenon because it plays an essential role in the exposure process of **E**xtreme **U**ltra**V**iolet (EUV) photoresists. The long mean free path of LEE can potentially reduce the resolution achieved in the lithography process (see chapter 6).

1.5 Other techniques to study low-energy electron interactions

For completeness, let us consider other techniques that are used to study the effects of LEE on materials. Early work to study LEE transmission of thin salt layers [8–10] and molecular layers [11], use a technique known as **L**ow-**E**nergy **E**lectron **T**ransmission spectroscopy (LEET) [5]. Here a thin layer material is deposited on a metal substrate. In LEET the total reflectivity is measured as well as the current that flows through the layer to the metal substrate. This is done as a function of incident electron energy. The interpretation of the data generated by this technique is challenging because the full current is measured, including secondary electrons. Another similar technique is **L**ow-**E**nergy **P**hoto **E**lectron **T**ransmission spectroscopy (LEPET) [5]. Here photoelectrons are generated from a metal layer on which the layer is deposited. All these techniques measure the transmission of a large surface without spatial resolution. **B**allistic **E**lectron **E**mission **M**icroscopy (BEEM) [12] is similar to the aforementioned techniques. However, BEEM is based on **S**canning **T**unneling **M**icroscopy (STM). A sharp metal tip placed close to the sample surface is used as the electron source. By scanning the surface with this tip, the electron transmission can be spatially resolved.

Other LEE transmission microscopy techniques have also been developed. Müllerová and Frank et al. [13–15] developed a SEM/STEM technique with very low-energy electrons. Here, a low-energy electron beam is focused to a spot on the sample. Both the reflected and transmitted electrons can be detected. An image of the sample can be formed by scanning the electron beam over the surface. As the incident electron energy can be accurately controlled, this also allows for spectroscopic measurements. In this technique, the specularly reflected electrons cannot be distinguished from secondary electrons and electrons that underwent inelastic scattering events.

Longchamp et al. have developed a low-energy electron holography technique in which the phase information is reconstructed without the use of any lenses in the imaging system [16]. The absence of lenses also means that the imaging system is free of any electron optical aberrations which allows for very high resolution imaging. They demonstrated that proteins can be imaged for a long time with an electron energy of 50 eV. They did not observe any evidence of radiation damage.

1.6 What to expect in eV-TEM

To describe the behaviour of LEE in a material it is not sufficient to describe the electron as a point charge that scatters via classical mechanics. Additionally, the assumption of weak electron scattering utterly fails to describe LEE dynamics. We find that the wavelike nature of electrons plays a very important role. At these low electron energies, interference effects and the band structure (which are closely related to each other) largely determine the electron reflectivity and transmissivity of the material.

We will focus on the case of multilayer graphene of which Müllerová et al. have shown that this is transparent enough for LEE to be used for electron microscopy in transmission [17]. First of all, because multilayer graphene is interesting by itself. The data presented in chapter 4 show the relation between LEE reflectivity and transmissivity and the unoccupied band structure. Second, we use multilayer graphene as a substrate for nanoscale objects in eV-TEM (chapter 3). To interpret these results, it is important that the substrate is well characterized. Here, we present two 'toy models' that qualitatively explain many of the features observed in the LEE transmission and reflection spectra we will present in chapters 4 and 5. The first model mainly focuses on the effects of elastic scattering, i.e. scattering without energy loss. The second model also allows us to study the effects of loss processes on the measured spectra.

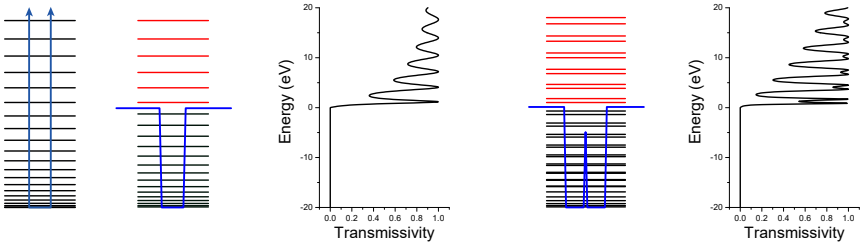

Figure 1.4: (a) Bound states of the infinite square well. **(b)** Spectrum of bound (black) and unbound states (red) of a single finite potential well. The unbound states in (b) have identical energy as the bound states that form in the infinite square well. **(c)** Transmission through the well. **(d)** Similar to (b), with two wells next to each other. The energy levels of (b) are split into two levels that straddle those in (b). **(e)** Transmission through a double well. The calculations were done with methods available in reference [18].

1.6.1 Quantum-well states

Let us first consider the case of double-layer graphene. The LEE transmission through two graphene layers is similar to the transmission of a finite square potential well*. This well represents the region between the two graphene layers, the interlayer region. This potential is described by:

$$V(x) = \begin{cases} 0 & \text{if } x < \frac{-L}{2} \\ -V_0 & \text{if } \frac{-L}{2} \leq x \leq \frac{L}{2} \\ 0 & \text{if } x > \frac{L}{2} \end{cases} \tag{1.3}$$

For energies < 0 eV, the solution of the Schrödinger equation with this potential is a series of discrete bound states (indicated by the black lines in figure 1.4b). For energies > 0 eV there is a continuous spectrum of *unbound* states of which the wave function extends over all of space and not just the well. These are the electron states we can use for microscopy. Since we do not include any loss processes in this simple model, current conservation gives us $T + R = 1$, where T and R are transmissivity and reflectivity of the potential

*This has been used to explain the reflectivity spectra of thin homogeneous metallic layers [19, 20].

well (i.e. the transmission and reflection probability). The reflectivity and transmissivity are thus each others complement. Unlike in classical mechanics, the transmissivity of the square well is not always equal to 1 when $E > 0$. The transmissivity of the finite potential well is plotted in figure 1.4c. The transmissivity is only equal to one for some energies. The transmissivity oscillates with increasing energy, reaching unity at the high-transmission resonances. We note that these resonances broaden with increasing energy. These maxima in the transmissivity (i.e minima in reflectivity) have identical energy as the bound states that form in the infinite potential well* [21, 22]. The finite square well therefore has a discrete series of unbound states. We refer to these states as high-transmission states (indicated by the red lines in figure 1.4b).

Next, we consider what happens when a third graphene layer is added. In triple-layer graphene there are two interlayer regions and the potential can thus be represented by two quantum wells in series. All the states seen for the single quantum well now split into two new states that straddle the energy of the state found in a single well (figure 1.4d). As more graphene layers are added, more states will appear. Eventually the spacing between the individual states is so small that they can no longer be distinguished and they merge into a continuous band.† At this point, multilayer graphene can be considered to be graphite. The band formed by the high transmission states is known as the interlayer band of graphite [23] (in the out-of-plane (Γ-A) direction in the band structure). The high-transmission resonances therefore correspond to unoccupied states in the graphene band structure. In chapter 4 we present a new technique (**A**ngle **R**esolved **R**eflection **E**lectron **S**pectroscopy, ARRES) to measure the full dispersion of the states that are part of the unoccupied band structure.

Note that the model presented here cannot explain all the features observed in the measured reflectivity and transmissivity spectra of multilayer graphene. The potential generated by multilayer graphene is more complicated than a square well. To explain the exact positions of the high-transmission states the three-dimensional potential should be taken into account [22]. In the next section we present a model with which we can investigate the effects of loss processes on the spectra.

*This is rooted in the fact that the cosine part of the unbound state is zero at these energies. The wave function is therefore zero at the boundaries and thus coincides with a solution of the infinite square well that has an infinite series of discrete (bound) states.

†The problem becomes equivalent to the Kronig-Penney model.

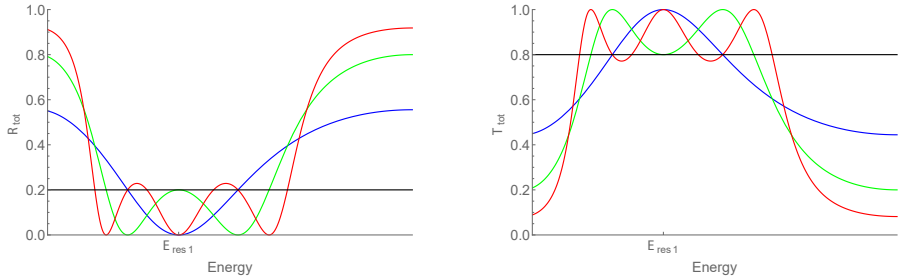

Figure 1.5: (a) Reflection, R_{tot}, and **(b)** transmission, T_{tot}, for one (black), two (blue), three (green) and four layers (red). Each layer, separately, has $R = 0.2$ and $T = 0.8$. This thus represents the no-loss situation with $R + T = 1$.

1.6.2 Effect of loss processes on LEE reflection and transmission spectra

In a slightly more sophisticated approach, we can use the transfer matrix method (explained in appendix A) to calculate the LEE reflectivity and transmissivity of a series of potential wells, as a first-order approximation to multilayer graphene. With the transfer matrix method we determine the total reflectivity and transmissivity, $R_{tot}(E)$ and $T_{tot}(E)$, of a combined system consisting of multiple layers. In this method the reflectivity and transmissivity, R and T, of each individual layer is considered while taking interference effects into account. The benefit of this method is that the effect of loss processes can easily be investigated by choosing R and T of each layer such that $R + T < 1$.

We first consider the no-loss situation with $R + T = 1$. The results of the model with $R = 0.2$ and $T = 0.8$, are shown in figure 1.5. Here $T_{tot}(E)$ (figure 1.5a) and $R_{tot}(E)$ (figure 1.5b) are shown for a single layer (black), two layers (blue), three layers (green), and four layers (orange). In the double-layer system, there is an energy at which $T_{tot} = 1$, a high-transmission state. For more than two layers, splitting of states into multiple states occurs, just as in the previous model (section 1.6.1). Interestingly, even though each layer in the multilayer systems has a transmissivity $T < 1$, the transmissivity of the combined system, T_{tot} is equal to one. For some energies, the transmissivity is higher than that of a single layer.

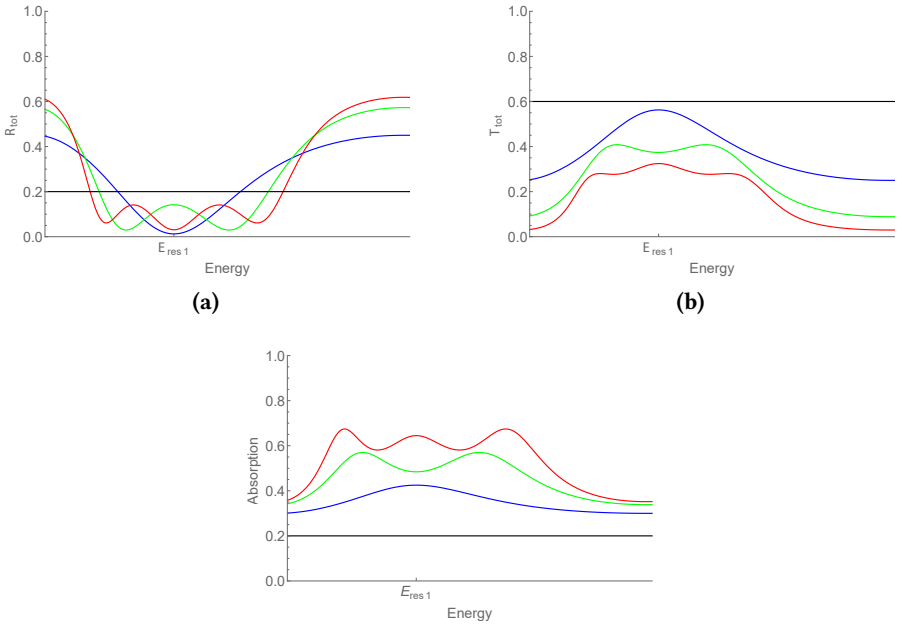

Figure 1.6: (a) Reflection, R_{tot}, and **(b)** transmission, T_{tot}, for one (black), two (blue), three (green) and four layers (red) for a system with loss. Each layer, separately, has $R = 0.2$ and $T = 0.6$. **(c)** $1 - R_{tot} - T_{tot}$, which gives the absorption of the total system.

In figure 1.6 we show the effect of losses when $R + T < 1$ in each layer. In this specific situation $R = 0.2$ and $T = 0.6$ for each layer. In figures 1.6a and 1.6b, we see that the high-transmission states are no longer 'full' transmission states. $T_{tot}(E)$ is always smaller than one. The high-transmission states are less pronounced than in the no-loss situation, especially in transmission.

In the no-loss situation, not only $R + T = 1$ also $R_{tot}(E) + T_{tot}(E) = 1$. This is not the case in the situation with loss. We can determine the loss of the total system by comparing $R_{tot}(E)$ and $T_{tot}(E)$ and see how much it deviates from unity:

$$S(E) = 1 - R_{tot}(E) - T_{tot}(E) \tag{1.4}$$

In figure 1.6c the total loss for different layer numbers is plotted. This shows that even though T and R of each individual layer do not depend on electron energy, the total loss of the system does (figure 1.6c). Most notably, the loss is highest at the resonance energies.

This model demonstrates the importance of interference effects on the transmission and reflectivity of the sample. When two identical layers are put together, the resulting combined system has properties that none of the individual layers have. To determine the properties of the constituents of a material, or the cross section of a certain process, the interference effects have to be taken into account. In chapter 5 we compare this model to our measurements.

At this point, let me give an outline of this dissertation.

1.7 Outline of this thesis

In this thesis we describe the development of a new type of transmission electron microscopy with very low-energy electrons, eV-TEM. eV-TEM is a microscopy (imaging) as well as a spectroscopy technique, i.e. we can use this to measure electron transmission as a function of energy. eV-TEM is incorporated in the ESCHER instrument which is a low-energy electron microscope (LEEM). Since we added an extra electron source, microscopy and spectroscopy can also be done in reflection.

In the first half of chapter 2 we explain how the imaging system of the ESCHER setup works, how the different imaging modes are used, and we explain how we designed the eV-TEM miniature low-energy electron source. In the second half of chapter 2 we give a detailed description of the sample preparation used for eV-TEM. This includes the preparation of samples with freestanding graphene or graphene oxide. Lastly, we present a description of how we deposit gold nanoparticles on graphene and DNA origami on graphene oxide.

In chapter 3 we explore the capabilities of eV-TEM as a microscopy technique by imaging freestanding graphene. We show that eV-TEM and LEEM (i.e transmission and reflection) can be used in parallel and present low-energy electron micrographs of the same region in both reflection and in transmission. We also show how graphene can be used as a sample holder for nanoscale objects. As an example we image graphene on which gold nanoparticles are deposited. We also image biological material: DNA origami deposited on graphene oxide. Here we find significant electron transmission through the DNA. This suggests that it is possible to perform quantitative spectroscopic experiments on biological material with low-energy electrons, and combine this with the high spatial resolution of the ESCHER microscope. Finally we determine the resolution of eV-TEM, in a non-aberration corrected imaging configuration, to be between 7 and 8 nm. This is somewhat better than expected for an uncorrected system, but not as good as expected for an optimized corrected system. We anticipate that improvements in sample alignment and optimization of the aberration correcting electron mirror settings will improve resolution to the 2-3 nm level.

By obtaining a sequence of micrographs at different energies, the energy dependent reflectivity and transmissivity can be determined. In chapter 4 we explore this spectroscopic capability of LEEM and eV-TEM. Spectroscopic measurements of multilayer graphene show resonances that are a consequence of high-transmission states in the material. These are manifested as minima in the reflectance spectrum. For the first time we now also measure these high-transmission states in transmission, where they appear as maxima in the transmissivity. We find that both the transmitted and the reflected signals decrease as the energy is increased. This indicates that inelastic effects play an important role in the interaction between low-energy electrons and the mate-

rial. Finally we demonstrate that the high-transmission states of multilayer graphene are part of the unoccupied band structure of multilayer graphene. We have developed a new technique called **A**ngle **R**esolved **R**eflection **E**lectron **S**pectroscopy (ARRES) to probe the unoccupied band structure of the material.

In chapter 5 we further investigate our finding in chapter 4 that both the reflected and transmitted signals decrease as the electron energy is increased. We do this by comparing the reflected and transmitted signal to determine the fraction of inelastically scattered electrons. We find that this 'scatter fraction' increases with electron energy, which is in line with expectations. We find that the universal curve (figure 1.2) is not really universal; interference effects strongly affect the transmissivity of the material. In addition to the LEEM and eV-TEM measurements, we present **E**lectron **E**nergy **L**oss **S**pectroscopy (EELS) data (also obtained with the ESCHER instrument).

In chapter 6 we study the effects of LEE on resists used in photolithography. The resists we investigate are poorly conducting. When these are illuminated with LEE, charge accumulates on the surface. The amount of charge on the surface depends on the conductivity and secondary electron emission of the resist. With LEEM we are able to accurately measure the surface potential that is generated by the charged surface. This allows us to measure the radiation-induced changes of material properties during the exposure with LEE. We find that charging-related phenomena play a significant role in the resist exposure. Such effects are not limited to the LEEM experiments. They are also important in industrial scale EUV lithography. In these circumstances the resist also accumulates charges as the high-energy-EUV photons (92 eV) generate photoelectrons that can leave the material. Our experiments allow us to quantify these effects, and to monitor radiation-induced changes in the resist down to 0 eV electron energy.

References

1. Abbe E. Beiträge zur Theorie des Mikroskops und der mikroskopischen Wahrnehmung. *Archiv für Mikroskopische Anatomie* **9,** 413–418 (1873).
2. Egerton R. F. Electron energy-loss spectroscopy in the TEM. *Reports on Progress in Physics* **72,** 016502 (2008).
3. Faruqi A. R. & Mcmullan G. Nuclear Inst . and Methods in Physics Research , A Direct imaging detectors for electron microscopy. *Nuclear Inst. and Methods in Physics Research, A* **878,** 180–190 (2018).
4. Seah M. & Dench W. Quantitative electron spectroscopy of surfaces: a standard data base for electron inelastic mean free paths in solids. *Surface and interface analysis* **1,** 2–11 (1979).
5. Naaman R. & Sanche L. Low-Energy Electron Transmission through Thin-Film Molecular and Biomolecular Solids. *Chemical Reviews* **107,** 1553–1579 (2007).
6. Tromp R., Hannon J., Ellis A., Wan W., Berghaus A. & Schaff O. A new aberration-corrected, energy-filtered LEEM/PEEM instrument. I. Principles and design. *Ultramicroscopy* **110,** 852–861 (2010).
7. Wolff P. A. Theory of secondary electron cascade in metals. *Physical Review* **95,** 56–66 (1954).
8. Hilsch R. Der Elektronenstoss an Kristallschichten zum Nachweis optischer Energiestufen. *Zeitschrift fur Physik* **77,** 427–436 (1932).
9. Wright D. A. Some effects of slow electron bombardment in thermionic valves. *British Journal of Applied Physics* **5,** 108–111 (1954).
10. Jacobs H., Greenberg I. N., Goble L. & Ramsa A. Resonance Potentials in Thin Films of Potassium Chloride. *Physical Review* **106,** 921–926 (1957).
11. Sanche L. Transmission of 0–15 eV monoenergetic electrons through thin-film molecular solids. *The Journal of Chemical Physics* **71,** 4860 (1979).
12. Kaiser W. J. & Bell L. D. Direct investigation of subsurface interface electronic structure by ballistic-electron-emission microscopy. *Physical Review Letters* **60,** 1406–1409 (1988).

13. Frank L., Hovorka M., Konvalina I., Mikmeková Š. & Müllerová I. Very low energy scanning electron microscopy. *Nuclear Instruments and Methods in Physics Research, Section A: Accelerators, Spectrometers, Detectors and Associated Equipment* **645,** 46–54 (2011).
14. Müllerová I., Hovorka M. & Frank L. A method of imaging ultrathin foils with very low energy electrons. *Ultramicroscopy* **119,** 78–81 (2012).
15. Müllerová I., Hovorka M., Konvalina I. & Unčovský M. Scanning transmission low-energy electron microscopy. *IBM Journal of Research and Development* **55,** 1–6 (2011).
16. Longchamp J.-N., Rauschenbach S., Abb S., Escher C., Latychevskaia T., Kern K. & Fink H.-W. Imaging proteins at the single-molecule level. *Proceedings of the National Academy of Sciences* **114,** 1474–1479 (2017).
17. Müllerová I., Hovorka M., Hanzlíková R. & Frank L. Very Low Energy Scanning Electron Microscopy of Free-Standing Ultrathin Films. *Materials Transactions* **51,** 265–270 (2010).
18. *NanoHUB* `https://nanohub.org/resources/pcpbt`.
19. Paggel J. J. Quantum-Well States as Fabry-Pérot Modes in a Thin-Film Electron Interferometer. *Science* **283,** 1709–1711 (1999).
20. Wu Y. Z., Schmid A. K., Altman M. S., Jin X. F. & Qiu Z. Q. Spin-dependent fabry-pérot interference from a Cu thin film grown on fcc Co(001). *Physical Review Letters* **94,** 1–4 (2005).
21. Merzbacher E. *Quantum Mechanics* Third edit. ISBN: 978-0-471-88702-7 (J. Wiley, 1970).
22. Feenstra R. & Widom M. Low-energy electron reflectivity from graphene: First-principles computations and approximate models. *Ultramicroscopy* **130,** 101–108 (2013).
23. Posternak M., Baldereschi A., Freeman A. J., Wimmer E. & Weinert M. Prediction of Electronic Interlayer States in Graphite and Reinterpretation of Alkali Bands in Graphite Intercalation Compounds. *Physical Review Letters* **50,** 761–764 (1983).